Supplementary Information for

Quasi-One-Dimensional Magnetism of Transition-Metal Oxide in Fe-Based Inorganic–Organic Hybrid Nanosheets

Takayuki Nakane*, Takashi Naka, Kazuyoshi Sato, Noriki Terada, Pascal Manuel, Ahmed Ibrahim, Shiro Kubuki, Chiya Numako, Dimitry Khalyavin, Anne de Visser, Hiroya Abe

Corresponding Author: Takayuki Nakane

NAKANE.Takayuki@nims.go.jp

Contents

SI-1 Fundamental information of HNS-1DFe

The solvothermal synthesis carried out in this study yielded a dark yellow powder as the product (HNS-1DFe), and scanning electron microscopy (SEM) observations confirmed that each grain was in the form of a nanosheet (see Fig. S1). Note that the observed nanosheets often transformed from unstable HNS-1DFe to a stable nanosheet during SEM observation at magnifications above 5000 times. Figure 1 (b) in the main text shows the sample after this transformation. Consequently, the main text estimates the thickness of HNS-1DFe to be about 50 ~ 100 nm; however, HNS-1DFe is likely thinner before transformation. HNS-1DFe is a precursor material for synthesizing Fe_3O_4 [S1], therefore, this transformed sample is considered to be Fe_3O_4 or a related material.

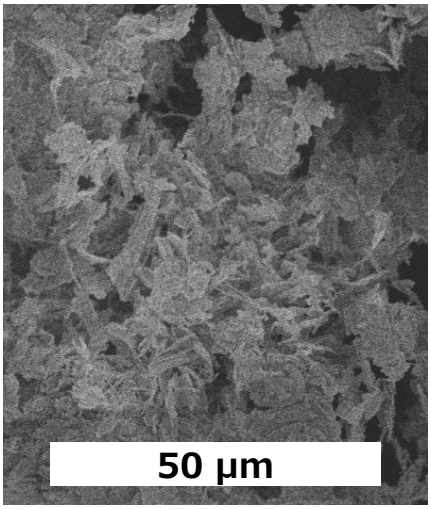

Fig. S1 SEM image of HNS-1DFe

The result of compositional analysis are listed in Table S-I. The amounts of K and Cl were also measured, since these elements were involved in the starting materials. Table S-I shows that the amounts of K and Cl are negligible. Therefore, the minimum chemical composition of HNS-1DFe is calculated to be $Fe_7(C_2H_4O_x)_9O_y$. The presence of a unit with the composition $C_2H_4O_x$ is

noteworthy. This indicates the existence of an organic component in HNS-1DFe and is consistent with the density ($d \approx 2.3 \sim 2.6$ g/cm^3) determined by a pycnometer with using Daphne7373 oil as the liquid medium. This value is considerably lower than that of iron oxides ($d > 5$ g/cm^3) and iron oxyhydroxides ($d \approx 4$ g/cm^3). Intuitively, the organic component $C_2H_4O_x$ seems to correlate with the ethylene glycol (EG), used as the solvent in the synthesis. The chemical composition of EG is $C_2H_4(OH)_2$, which often acts as $(C_2H_4O_2)^{2-}$ in complex or related solid materials. Thus, an x value of 2 is speculated and the y value is calculated to be $y \approx 4.77$. Note that the oxygen content was not calculated directly from measured values but inferred from the residual fraction of the compositional analysis, the accuracy is not high.

Table S-I. Chemical composition and molar ratio obtained by inductively coupled plasma mass spectroscopy (ICP) and organic elemental analysis (OEA) of HNS-1DFe.

composition	Fe	C	H	K	Cl	O
wt%	38.65	21.37	3.56	0.21	0.19	36.02
mol%	0.692	1.779	3.560	0.005	0.005	2.251

* The weight percentage of oxygen was calculated as the remaining value from the sum of the ratios of the other elements: 36.02 = 100 - 38.65 - 21.37 - 3.56 - 0.21 - 0.19.

SI-2 Analysis of Mössbauer spectra of HNS-1DFe

Figure 2 (b) in the main text reports the temperature dependence of the Mössbauer spectra for Fe in HNS-1DFe. The analysis of these spectra yields the results listed in Table S-II. Here, the isomer shift, δ, the quadrupole splitting, Δ, of Fe and the line width, Γ, are listed as functions of temperature. No evidence of multiple Fe valence states was identified in the spectra in Fig. 2 (b), and all Fe ions are 3+ with $S = 5/2$. This is consistent with the result of the XANES spectrum.

Table S-II. Isomer shift (δ), quadrupole splitting (Δ), and line width (Γ) of Mössbauer spectra measured for HNS-1DFe.

T (K)	δ (mm/s)	Δ (mm/s)	Γ (mm/s)
294.2	0.316	0.657	0.347
100.7	0.422	0.654	0.444
40.7	0.420	0.488	0.448

On the other hand, the temperature dependence of the recoil-free fraction, f, of the Mössbauer nucleus can be expressed by the formula

$$f = \exp\left[-\left(\frac{3E_R}{2k_B\Theta_D}\right)\left\{1 + 4\left(\frac{T}{\Theta_D}\right)^2 \cdot \int_0^{\Theta_D/T} \frac{x}{e^x - 1} \cdot dx\right\}\right]$$

, where E_R, k_B, and Θ_D are recoil energy (=19.6 keV), Boltzmann's constant, and the Debye temperature, respectively [S2]. Because the value of f can be approximated by the absorption area,

A, of the Mössbauer spectrum, Θ_D can be determined by plotting A against temperature. Figure S2 shows this plot for HNS-1DFe. In this case, Θ_D was evaluated as 246(33) K for Fe in HNS-1DFe. This value is smaller than the previously reported Θ_D values for α-Fe_2O_3 (= 324(45) K) and γ-Fe_2O_3 (= 300(24) K) [S3]. These results indicate that Fe in HNS-1DFe is more weakly bound in the crystal structure compared with Fe in α-Fe_2O_3 and γ-Fe_2O_3, which posess 3D corundum and inverse spinel structures, respectively. This is attributed to the 1D structure of the iron oxide matrix in HNS-1DFe.

Finally, no peak splitting associated with the appearance of a hyperfine structure was observed, despite the cooling of the sample below 120 K. This indicates that Fe in HNS-1DFe is not affected by the internal magnetic field of a ferromagnetic component in this temperature region. This observation provides important evidence regarding the magnetic purity of HNS-1DFe.

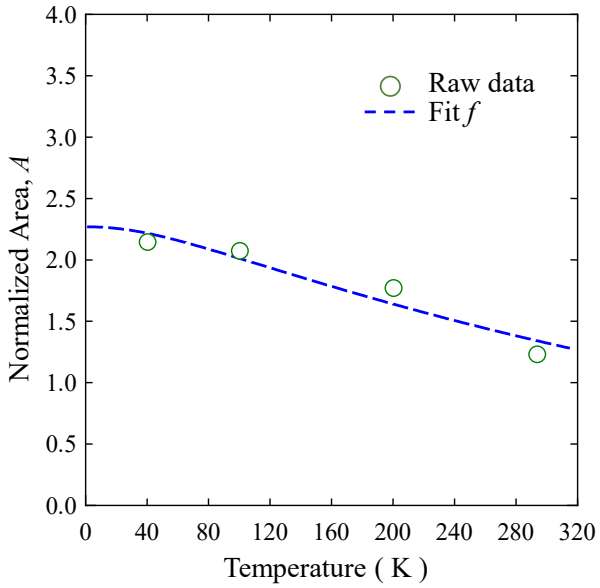

Fig. S2 Relationship between the normalized Mössbauer spectrum area, A, and temperature. The dashed line represents the calculated values of A.

SI-3 Magnetic susceptibility of HNS-1DFe

Figure S3 (a) shows the temperature dependence of the magnetic susceptibility, $\chi(T)$, of HNS-1DFe in applied fields of 0.1 kOe measured after field cooling (FC) and zero-field cooling (ZFC). The FC data above about 21 K are almost identical to the FC 10 kOe data reported in Fig. 3 (a) in the main text. The kink at 21 K can be identified as the magnetic transition temperature. A drastic change is not observed in the magnitude of the susceptibility below and above the transition temperature. Therefore, the magnetic ordering of this spin system is antiferromagnetic (AF) nature, rather than ferromagnetic. On the other hand, two characteristic splitting temperatures are observed between the $\chi(T)$ curves of ZFC and FC data.

First, the $\chi(T)$ curves of ZFC and FC data in 0.1 kOe split below the transition temperature at 21 K. Figure S3 (b) shows the thermoremanent magnetization (TRM) measured after FC under an activation field of 0.1 kOe. Near 21 K, the TRM increases suddenly, with a transition to a weakly first-order canted AF state. This suggests that a small spontaneous magnetization emerges below the magnetic transition, which may be attributable to a macroscopically canted AF order below 21 K.

Next, we discuss the small step-like anomaly at around 120 K in $\chi(T)$ measured under ZFC conditions in 0.1 kOe. It is important to note that a similar small step is not observed in the $\chi(T)$ measured under FC conditions in 0.1 kOe and 10 kOe. The TRM signal appears below 120 K, and further cooling reveal a tendency toward saturation at a value of $\sim 1.5\times10^{-4}$ emu/g (2.2×10^{-2} emu/mol_{Fe}) at 40 K. Therefore, differences in long-range magnetic ordering with respect to the anomaly at around 120 K were examined using the Mössbauer spectra. According to Fig. 2 (b) in the main text, no peak splitting indicative of a hyperfine structure was observed, upon cooling the

sample to 40.7 K. This indicates that the Fe in HNS-1DFe is not affected by the internal magnetic field associated with the ferromagnetic-like component of the magnetic response in this temperature region. These results indicate that the magnetic anomaly at 120 K in Fig. S3 (a) originates from a minor secondary phase in the examined sample. A plausible candidate for this secondary phase is Fe_3O_4, which undergoes a Verwey transition near 120 K [S4], given that HNS-1DFe serves as a precursor for the synthesis of magnetite particles [S1].

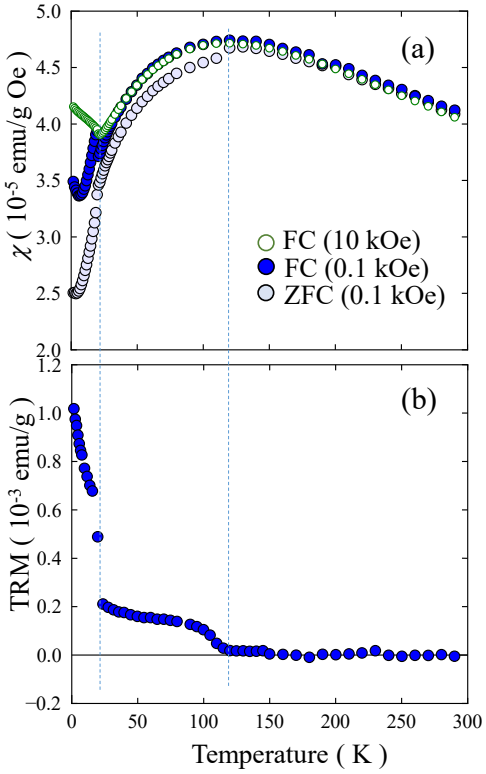

Fig. S3 Magnetic behaviour of HNS-1DFe. (a) Temperature dependence of the magnetic susceptibility. (b) Thermoremanent magnetization of the same sample.

SI-4 Calculation procedure for the lattice contribution to the specific heat of HNS-1DFe

In analyzing the specific heat data, two major contributions are assumed: the magnetic contribution, C_{mag}, from the spin system, and the lattice contribution, $C_{lattice}$, due to lattice vibrations (phonons). To determine C_{mag}/T the lattice contribution is substracted as $C_{mag}/T = [C_{mol} - C_{lattice}]/T$. Here, C_{mol} is the measured specific heat. For evaluating $C_{lattice}$, we basically follow the procedure used for aluminate oxides [S5-S7].

The spectroscopic data from Fourier transform infrared (FT-IR) spectroscopy (see Fig. 1 (c) in the main text) show that the partial phonon density of states (PDOS) for the heavy Fe ions in HNS-1DFe is distributed mainly below 400 cm^{-1}, whereas the partial PDOS for the light oxygen and carbon ions is distributed above 400 cm^{-1}, and that for hydrogen is distributed above 2700 cm^{-1}. At low frequencies, the PDOS exhibits a Debye-type parabolic frequency dependence consisting mainly of contributions from Fe^{3+} ions. In the case of spinel oxides [S5, S6], the Einstein–Debye (ED) model was employed to obtain $C_{lattice}$. The obtained Debye and Einstein temperatures associated with the lattice degrees of freedom (LDFs) of theconstituent elements are consistent with the PDOS of isostructural spinel oxides [S7]. For the pseudo-molecule $Fe_7O_5(C_2H_4O_2)_9$, we fitted C_{mol}/T at high temperatures ($T >> T_C$) to the ED function to obtain $C_{lattice}$ as well the Debye and Einstein temperatures. The ED function,

$$C_{ED} = 3Ra_D x_D^{-3} \int_0^{x_D} \frac{x_D^4 e^{x_D}}{(e^{x_D}-1)^2} dT + R \sum_{k=1}^{3} a_i \frac{x_i^2 e^{x_i}}{(e^{x_i}-1)^2}$$

consists of two terms and makes use of four fitting parameters: the Debye temperature Θ_D and the Einstein temperatures Θ_{E1}, Θ_{E2}, and Θ_{E3}. The LDFs of the elements (Fe, C, and O) in HNS-1DFe

are distributed among one acoustic and three optical modes. Here, $x_i = \Theta_i/T$ ($i = D$, E_1, E_2, and E_3) are the reduced inverse temperatures, a_i is the number of LDFs, and R is the gas constant. The Dulong–Petit rule predicts that, in a three-dimensional lattice, the molar specific heat is $3rR$, which is reproduced asymptotically by the ED function at high temperatures ($T >> \Theta_D$, Θ_{E1}, Θ_{E2}, and Θ_{E3}), where r is the number of atoms per formula unit. The factor $3r = 3\times84$ represents the number of LDFs in HNS-1DFe. Here, we assume that the contribution of hydrogen atoms can be ignored because the characteristic temperature of the phonon mode associated with hydrogen, namely Θ_{E3}, is much greater than the experimental temperature window; consequently, the corresponding specific-heat contribution might be diminished in the present measurement conditions. Indeed, the intense FT-IR and Raman modes associated with hydrogen occur above 2700 cm^{-1}. If we assume Θ_{E3} = 3000 K for hydrogen motion in HNS-1DFe, the optical contribution of hydrogen to the specific heat is less than 1 % of the total lattice contribution $C_{lattice}$ at T = 300 K. A fairly good fit is obtained to the ED function above 100 K (see Fig. S4). The obtained Debye and Einstein temperatures are listed in Table S-III, together with several other defined parameters defined in this fitting procedure. We conclude that the obtained Debye temperature for iron (≈ 237 K) is consistent with the value (≈ 245 K) calculated from the Mössbauer experiment (see SI-2).

Table S-III. Composition, lattice degrees of freedom a_i (i = D, E_1, E_2, and E_3), and Debye and Einstein temperatures Θ_i of HNS-1DFe with the chemical composition of $Fe_7O_5(C_2H_4O_2)_9$.

mode	composition	a_i^*	mode	Θ_i (K)
Fe	7	3	D	237
O	23	9.86	E_1	318
C	18	7.71	E_2	1342
H	36	15.43	E_3	–

* Note that a_i is normalized by the composition of Fe.

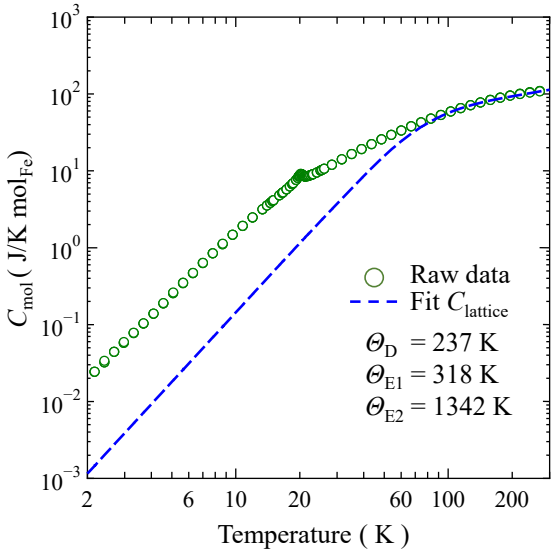

Fig. S4 Specific heat of HNS-1DFe as a function of temperature. The dashed line represents the calculated lattice component with characteristic temperatures obtained from the specific heat above 100 K (see text). Note that the unit of specific heat is per mole of Fe.

SI-5 Raw data of diffraction patterns for FeO-1DHNS

For the acquisition of relevant information about the crystal structure of HNS-1DFe, powder X-ray diffraction (XRD) and Powder Neutron diffraction (PND) measurements were performed. Figure S5 shows the resulting raw data. There are two PND data sets, since the measurements were conducted using two different detectors to collect a wide range of diffraction data. The most striking feature in the data is the prominent intense main peak, which is considered a typical characteristic of a hybrid material containing organic molecules. However, several tiny peaks originating from the crystal structure can be detected as well. The background was carefully removed to better visualize these tiny peaks and carry out a structural analysis.

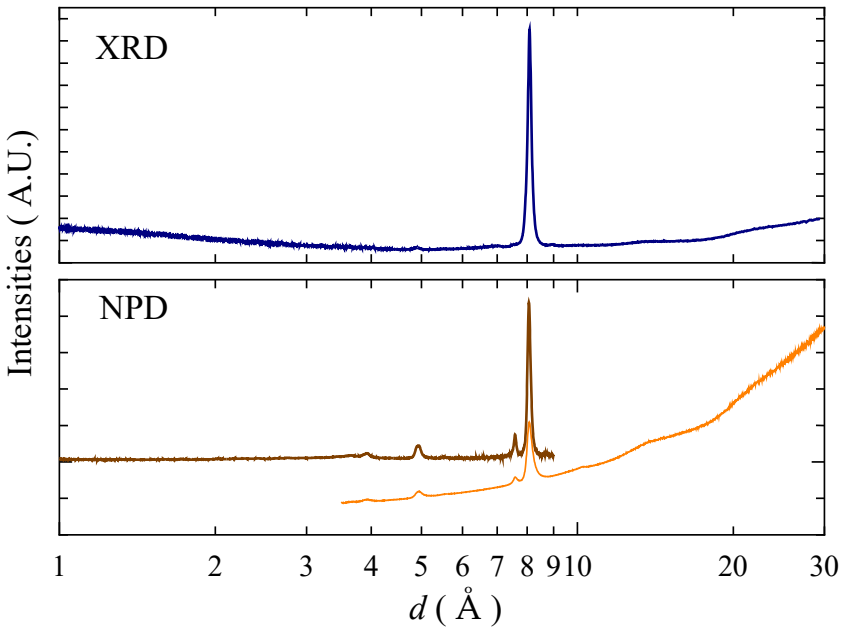

Fig. S5 Raw diffraction patterns plotted against the lattice distance, *d*, of XRD and PND measurements for HNS-1DFe. Two PND patterns are due to different set points (see main text).

The extremely intense peak is observed at $d \approx 8.05$ Å in both diffraction patterns. This peak is considered to originate from the iron oxide matrix in HNS-1DFe, and we can find the same index member of this peak (see red line in Fig. 4 (a) in the main text). However, we cannot identify these peaks clearly in the PND data, except for the main peak. The reason for this is not clear, but most likely relates to the difference between the scattering factors of XRD and the scattering amplitudes of PND.

REFERENCES

S1. H. Abe, T. Naka, K. Sato, K. Suzuki and M. Nakano, Shape-Controlled Syntheses of Magnetite Microparticles and Their Magnetorheology, *Int. J. Mol. Sci.*, **20**, 2019, 3617-3627.

S2. A.Vertes and Z. Homonnay, *Mössbauer Spectroscopy of Sophisticated Oxides*. (Akademiai Kiado, 1997)

S3. A. Ibrahim, K. Tani, K. Hashi, B. Zhang, Z. Homonnay, E. Kuzmann, A. Bafti, L. Pavić, S. Krehula, M. Marciuš and S. Kubuki, Debye Temperature Evaluation for Secondary Battery Cathode of α-$Sn_xFe_{1-x}OOH$ Nanoparticles Derived from the ^{57}Fe- and ^{119}Sn-Mössbauer Spectra, *Int. J. Mol. Sci*., **25**, 2025,2488-2513.

S4. E. J. W. Verwey, Electronic Conduction of Magnetite (Fe_3O_4) and its Transition Point at Low Temperatures, *Nature*, **144**, 1939, 327-328.

S5. N. Tristan, J. Hemberger, A. Krimmel, H. A. K. von Nidda, V. Tsurkan and A. Loidl, Geometric frustration in the cubic spinel MAl_2O_4 (M = Co, Fe, and Mn), *Phys. Rev. B*, **72**, 2005, 174404.

S6. T. Naka, T. Nakane, S. Ishii, M. Nakayama, A. Ohmura, F. Ishikawa, A. de Visser, H. Abe and T. Uchikoshi, Cluster glass transition and relaxation in the random spinel $CoGa_2O_4$, *Phys. Rev. B*, **103**, 2021, 224408.

S7. S. López-Moreno, P. Rodróguez-Hernández, A. Muňoz, A. H. Romero, F. J. Manjón, D. Errandonea, E. Rusu and V. V. Ursaki, Lattice Dynamics of $ZnAl_2O_4$ and $ZnGa_2O_4$ under High Pressure, *Ann. Phys. (Berlin)*, **523**, 2011, 157-167.